

1 **External forcing explains recent decadal variability of the ocean carbon sink**

2

3 Galen A. McKinley¹, Amanda R. Fay¹, Yassir A. Eddebar², Lucas Gloege¹,
4 Nicole S. Lovenduski³

5

6 **Affiliations:** ¹Lamont Doherty Earth Observatory / Columbia University, Palisades NY. ²Scripps
7 Institution of Oceanography, La Jolla, CA. ³University of Colorado Boulder, Boulder, CO.

8 *Corresponding author: Email: mckinley@ldeo.columbia.edu

9

10

11 Key points:

- 12 • The reduced ocean carbon sink in the decade of the 1990s can be explained by the slowed
13 growth rate of atmospheric CO₂.
- 14 • The global sea surface temperature response to Mt Pinatubo in 1991 explains the intra-
15 decadal pattern of the ocean carbon sink in the 1990s.
- 16 • There will be an immediate reduction in ocean carbon uptake as atmospheric pCO₂
17 responds to cuts in anthropogenic emissions.

18 **The ocean has absorbed the equivalent of 39% of industrial-age fossil carbon emissions,**
19 **significantly modulating the growth rate of atmospheric CO₂ and its associated impacts**
20 **on climate. Despite the importance of the ocean carbon sink to climate, our**
21 **understanding of the causes of its interannual-to-decadal variability remains limited.**
22 **This hinders our ability to attribute its past behavior and project its future. A key period**
23 **of interest is the 1990s, when the ocean carbon sink did not grow as expected. Previous**
24 **explanations of this behavior have focused on variability internal to the ocean or**
25 **associated with coupled atmosphere/ocean modes. Here, we use an idealized upper ocean**
26 **box model to illustrate that two external forcings are sufficient to explain the pattern and**
27 **magnitude of sink variability since the mid-1980s. First, the global-scale reduction in the**
28 **decadal-average ocean carbon sink in the 1990s is attributable to the slowed growth rate**
29 **of atmospheric pCO₂. The acceleration of atmospheric pCO₂ growth after 2001 drove**
30 **recovery of the sink. Second, the global sea surface temperature response to the 1991**
31 **eruption of Mt Pinatubo explains the timing of the global sink within the 1990s. These**
32 **results are consistent with previous experiments using ocean hindcast models with and**
33 **without forcing from variable atmospheric pCO₂ and climate variability. The fact that**
34 **variability in the growth rate of atmospheric pCO₂ directly imprints on the ocean sink**
35 **implies that there will be an immediate reduction in ocean carbon uptake as atmospheric**
36 **pCO₂ responds to cuts in anthropogenic emissions.**

37

38 Plain Language Summary

39 Humans have added 440Pg of fossil fuel carbon to the atmosphere since 1750, driving up the
40 atmospheric CO₂ concentration. But not all of this carbon remains in the atmosphere. The
41 ocean has absorbed 39%, substantially mitigating anthropogenic climate change. Though this
42 “ocean carbon sink” is a critical climate process, our understanding of its mechanisms remains
43 limited. Of great interest is the unexplained slow-down of the ocean carbon sink in the 1990s
44 and a subsequent recovery. In this work, we use a simple globally-averaged model to show
45 that two processes external to the ocean are sufficient to explain the slowing of the ocean
46 carbon sink in the 1990s. First, a reduced rate of accumulation of carbon in the atmosphere
47 after 1989 reduced the atmosphere-ocean gradient that drives the ocean sink. Second, the
48 eruption of Mt Pinatubo led to changes in ocean temperature that modified the timing of the
49 sink from 1991 to 2001. We illustrate that the most important control on the decade-averaged
50 magnitude of the ocean sink is variability in the growth rate of atmospheric CO₂. This implies
51 that as future fossil fuel emission cuts drive reduced growth of atmospheric CO₂, the ocean
52 sink will immediately slow down.

53

54

55

56

57 **1. Introduction**

58 The ocean has absorbed the equivalent of 39% of fossil carbon emissions since 1750, significantly
59 modulating the growth of atmospheric CO₂ and the associated climate change (Friedlingstein et
60 al. 2019; Le Quéré et al., 2018a,b; McKinley et al., 2017; Ciais et al., 2013). This sink is expected
61 to grow and substantially mitigate atmospheric carbon accumulation for the next several centuries
62 (Randerson et al., 2015). Yet, we lack a detailed understanding of spatial and temporal variability
63 in the sink and its underlying mechanisms. Incomplete understanding of ocean flux variability
64 contributes to significant uncertainty in the global anthropogenic carbon budget for recent decades;
65 this uncertainty is equivalent to ~10% of the atmospheric pCO₂ growth rate (Friedlingstein et al.
66 2019; Le Quéré et al., 2018a,b). This imbalance, in turn, limits the scientific community's ability
67 to inform international efforts to curb fossil fuel emissions (Peters et al., 2017).

68 Recent studies have concluded that ocean hindcast models, which have long been used to assess
69 the ocean sink, may significantly underestimate its variability (Gruber et al., 2019a; Le Quéré et
70 al., 2018b). These conclusions are based on comparisons to new observation-based gap-filled
71 products that suggest substantially larger interannual to decadal variability (Landschützer et al.,
72 2015, 2016; Rödenbeck et al., 2013, 2015). It is possible, however, that these gap-filled products
73 do not accurately represent the surface ocean carbon cycle given that their raw input data cover
74 only 1.5% of the global ocean in the last 3 decades, and only 3.5% in the most recent years (Bakker
75 et al., 2016). Variability may be amplified by the significant extrapolation that occurs when global
76 full-coverage maps are produced from these very sparse data (Fay et al., 2018; Rödenbeck et al.,
77 2015).

78 The ocean carbon sink of the 1990s is of particular interest. During this time, the growth of the
79 ocean sink stalled from its expected growth (DeVries et al., 2019; Fay and McKinley, 2013;
80 Landschützer et al., 2015; Le Quéré et al., 2007; Lovenduski et al., 2008). Using a data-constrained
81 ocean circulation model, it has been suggested that this slow-down was caused by excess
82 outgassing of natural carbon due to an anomalously strong overturning of the ocean's upper 1000m
83 (DeVries et al., 2017). Changing patterns of wind-driven circulation in the Southern Ocean have
84 also been proposed (Gruber et al., 2019a; Landschützer et al., 2015). Consensus has yet to be
85 achieved on the mechanisms driving changes in the 1990s sink. It is critical that we accurately
86 quantify and diagnose this variability so that we can better project the future ocean carbon sink
87 and, thus, the degree to which the ocean carbon sink will continue to mitigate global climate
88 change.

89 **2. Methods**

90 In this study, we compare the ocean carbon sink since 1980 as estimated from six ocean hindcast
91 models, four observationally-based products, and a theoretical upper ocean box model. We
92 supplement our analysis with results from nine ocean hindcast models run in constant climate
93 model (DeVries et al., 2019). Supporting information provides additional methodological details.

94 **2.1 Models and Products**

95 Six (6) ocean hindcast models for 1980-2017 are the primary basis for this analysis (Table S1).
96 Ocean hindcast models are gridded, three dimensional representations of the evolution of the ocean
97 state for recent decades. These models have been forced at the surface by winds, heat and buoyancy
98 fluxes from reanalyses of the past atmospheric state. The models we analyze are those used in the
99 recent versions of the Global Carbon Budget (Le Quéré et al., 2018a,b).

100 Four (4) observationally-based products are also utilized, chosen because they all cover 1985-2016
101 (Table S2). While models have full coverage in space and time, in situ observations only cover a
102 small fraction of the global surface ocean. These observation-based products utilize gap-filling
103 techniques to estimate values in all periods and areas not directly observed. Interpolation methods
104 fill spatial and temporal gaps by assuming statistical relationships with neighboring or similar areas
105 with available observations.

106 Ensemble means of the 4 observationally-based products and the 6 hindcast models are calculated.

107 **2.2 Flux analysis**

108 Model fluxes span years 1980-2017, while observationally-based products span the 1985-2016
109 period (Table S1, S2). An area-weighted annual mean timeseries is calculated for each model and
110 product for regions of interest: i) global, ii) east equatorial Pacific biome (Fay & McKinley, 2014),
111 and iii) global, excluding east equatorial Pacific biome. We note that individual models and
112 products utilize different methods for the flux calculation, including wind speed products and
113 parameterizations. The standard approach of our field is to use the mean of these estimates as the
114 current best-estimate of the air-sea flux (DeVries et al., 2019; Le Quéré et al., 2018a,b).

115 **2.3 pCO₂ analysis**

116 For pCO₂, hindcast models span 1980-2017, while observationally-based products cover 1985-
117 2016. Detrended pCO₂^{ocean} is obtained by removing the atmospheric trend of 1.70 μatm/yr (the
118 observed average annual atmospheric pCO₂ change for 1980 to 2017) from each time series.
119 ΔpCO₂ is calculated at annual timescales by surface ocean pCO₂ - atmospheric pCO₂ [ΔpCO₂ =
120 pCO₂^{ocean} - pCO₂^{atmosphere}].

121 **2.4 Accounting for open ocean areas without observationally-based estimates**

122 There are large differences in the spatial extent of the observationally-based products compared to
123 the hindcast models. This difference, when left unaccounted for, results in significant discrepancies
124 between models and products for both global mean flux and global mean pCO₂. We correct for
125 spatial coverage differences by calculating the mean flux or mean pCO₂ in the area of each model
126 where there is no coverage for a specific data product. By calculating this offset from 6 models for
127 each individual data-product's spatial coverage, we generate a product-specific offset for the
128 annual time series that corrects for the difference in spatial coverage. As expected, observationally-
129 based products with more complete spatial coverage have smaller offsets (Table S2). The only
130 exception to this data-product correction process is the JENA product (Rödenbeck et al., 2013)
131 because it is produced with full spatial coverage and is primarily used in this analysis on its coarser
132 native grid.

2.5 Upper Ocean Box Model

The box model (Fig S1) solves for the time change of Dissolved Inorganic Carbon (DIC) in single upper ocean box (Equation 1).

$$\frac{dDIC}{dt} = \frac{v}{V} (DIC_{\text{deep}} - DIC) - \frac{k_w S_o \rho}{dz} (pCO_2^{\text{ocean}} - pCO_2^{\text{atmosphere}}) \quad (1)$$

The first term on the right of Equation 1 is the overturning circulation (v) acting on the surface to depth gradient of DIC. V is the volume of the global ocean box, $V = A * dz$. Our value for the global area removes ice-covered regions. The second term on the right of Equation 1 is the air-sea exchange of CO_2 . The rate of flux is set by a piston velocity (k_w), solubility (S_o) and density (ρ) over the depth of the box ($dz = 200m$), multiplied by the ocean to atmosphere difference of pCO_2 (Wanninkhof, 2014). S_o and pCO_2^{ocean} are calculated using full carbon chemistry (Dickson and Millero, 1987; Mehrbach et al., 1973) given inputs of temperature, salinity, alkalinity and DIC. Parameters choices are globally representative values outside the tropics (Table S3). Consistent with current understanding of the drivers of ocean uptake of anthropogenic carbon (Gruber et al., 2019b), the biological pump is assumed constant over time. This leads to our abiotic formulation. Thus, we remove from the DIC_{deep} concentration the amount of carbon that would be vertically supplied, and then removed biologically. We take a global mean DIC_{deep} concentration of 2320 $mmol/m^3$ and a biological pump component of this of 265 $mmol/m^3$ (Sarmiento and Gruber 2006, Table 8.2, Figure 8.4.2, organic + carbonate) leading to $DIC_{\text{deep}} = 2055 \text{ mmol/m}^3$.

NOAA ESRL surface marine boundary layer annual mean observed $xCO_2^{\text{atmosphere}}$ is used to force the model. This is the same $xCO_2^{\text{atmosphere}}$ data used to force the ocean hindcast models and observationally-based products, and in conversion to $pCO_2^{\text{atmosphere}}$, the water vapor correction is applied. $pCO_2^{\text{atmosphere}}$ is interpolated linearly to monthly resolution, using the annual mean value at the mid-point of each year. Temperature is held at a constant global surface ocean value, except if the impact of volcanoes is included (Fig. S2). This estimate of the forced sea surface temperature (SST) response to the El Chichon and Mt Pinatubo volcanic eruptions is based on the Community Earth System Model Large Ensemble (CESM LENS) (Eddebbar et al., 2019). The global-mean expression of this forced temperature anomaly extends to several hundred meters depth in CESM LENS. The box model is time stepped with monthly resolution for 1959-2018. In all cases, the box model is spun up from 1959-1979 using observed $pCO_2^{\text{atmosphere}}$ and the values presented in Table S3.

The mean uptake flux in the box model is most sensitive to the depth of the box and the global overturning rate (Fig S3, Supporting Information). We use $dz = 200m$ and set other parameters to result in a mean flux and ΔpCO_2 consistent with the ocean models and observationally-based products.

3. Results/Discussion

Global air-sea CO_2 flux variability estimated by the ensemble means of ocean hindcast models and of observationally-based products (Gruber et al., 2019a; Landschützer et al., 2016) are highly correlated ($r = 0.95$) (Fig 1a, Table S4). The decadal variability of the air-sea CO_2 flux is not driven by a single region, but instead is largely globally coherent (DeVries et al., 2019; Le Quéré et al., 2018b). This air-sea CO_2 flux is primarily determined by the difference of the surface ocean and

177 the atmosphere $p\text{CO}_2$, $\Delta p\text{CO}_2 = p\text{CO}_2^{\text{ocean}} - p\text{CO}_2^{\text{atmosphere}}$ (Fay & McKinley, 2013; Landschützer
178 et al., 2015; Lovenduski et al., 2007; McKinley et al., 2017) with a more negative $\Delta p\text{CO}_2$ driving
179 a greater ocean uptake. From 1991 to 1993, $\Delta p\text{CO}_2$ experiences a negative or neutral anomaly on
180 the global average and at most latitudes over the 91% of ocean that is south of 45°N (Fig 2, S3).
181 From 1993-1995 and again for 1999-2001, $\Delta p\text{CO}_2$ anomalies were positive at most latitudes. In
182 1997-1998, the El Niño event drove negative $\Delta p\text{CO}_2$ anomalies in the tropics (Fig 2), but the El
183 Niño-Southern Oscillation (ENSO) cycle does not dominate the global mean decadal variability
184 (Fig 2, Fig S5). Following 2001, $\Delta p\text{CO}_2$ anomalies become much more negative at all latitudes
185 outside the tropics and in the global average (Fig 2).

186 From 1980 to 2017, $p\text{CO}_2^{\text{atmosphere}}$ increased from $330 \mu\text{atm}$ to $394 \mu\text{atm}$, and $p\text{CO}_2^{\text{ocean}}$ follows the
187 atmosphere on the long-term (Fig 3a). Detrending reveals the detailed features of these timeseries
188 (Fig 3b). Growth of $p\text{CO}_2^{\text{atmosphere}}$ slowed significantly with respect to the long-term trend starting
189 in the late 1980s (Fig 3b, Sarmiento 1993). This change was due in part to a pause of growth in
190 fossil fuel emissions from 1989 to 1994 when fossil fuel emissions were approximately constant
191 at 6.1 Pg/yr (Friedlingstein et al. 2019; Sarmiento et al., 2010). Increased uptake of carbon by
192 the terrestrial biosphere also contributed significantly to this slow down (Brovkin et al., 2010;
193 Sarmiento et al., 2010; Angert et al., 2004). Though some studies have attributed the increased
194 land carbon sink to temperature and radiation changes caused by Mt. Pinatubo's 1991 eruption,
195 there is not a consensus with respect to the mechanisms on land (Frölicher et al., 2011; Brovkin et
196 al., 2010; Sarmiento et al., 2010; Angert et al., 2004; Lucht et al., 2002).

197 Deviations in the evolution of $p\text{CO}_2^{\text{ocean}}$ from the evolution of $p\text{CO}_2^{\text{atmosphere}}$ drive $\Delta p\text{CO}_2$ changes
198 in the observationally-based products and hindcast models (Fig 3c). Since global mean $\Delta p\text{CO}_2$ is
199 only $\sim 5 \mu\text{atm}$ (Fig 3c), anomalies of a few μatm in either $p\text{CO}_2^{\text{atmosphere}}$ or $p\text{CO}_2^{\text{ocean}}$ can
200 significantly impact the air-sea CO_2 flux. In 1992, growth of $p\text{CO}_2^{\text{ocean}}$ abruptly slowed in both the
201 hindcast models and the observationally-based products (Fig 3b) and $\Delta p\text{CO}_2$ becomes more
202 negative (Fig 3c). From 1992 through 2001, $p\text{CO}_2^{\text{ocean}}$ increases more rapidly than $p\text{CO}_2^{\text{atmosphere}}$,
203 driving a positive change in $\Delta p\text{CO}_2$ over this period (Fig 3c). For 2002-2011 and beyond, $p\text{CO}_2^{\text{ocean}}$
204 grows more slowly than the strongly accelerating $p\text{CO}_2^{\text{atmosphere}}$, leading to increasingly negative
205 $\Delta p\text{CO}_2$ over 2002-2011 (Fig 3c).

206 Given that global mean changes in the ocean sink (Fig 1) are found to occur at most latitudes (Fig
207 2), we hypothesize an important role for external forcing. To explore these drivers, we apply the
208 upper ocean box model (Fig S1). The key processes captured by this model are (1) ventilation to
209 the surface of deep waters with low anthropogenic carbon content, and (2) air-sea gas exchange.
210 First, we ask: Are the changes in the growth rate of $p\text{CO}_2^{\text{atmosphere}}$ (Fig 3a,b) sufficient to
211 substantially modify the global ocean carbon sink?

212 To test this, the box model is forced only with changes in the observed $p\text{CO}_2^{\text{atmosphere}}$. When the
213 growth rate of $p\text{CO}_2^{\text{atmosphere}}$ slows in the late 1980s, growth of $p\text{CO}_2^{\text{ocean}}$ gradually slows in
214 response (Fig 3b, red dashed line). $p\text{CO}_2^{\text{ocean}}$ achieves a few years after the $p\text{CO}_2^{\text{atmosphere}}$ minimum
215 in 1994, consistent with the long equilibration timescale for carbon due to carbonate chemistry
216 (Fig S6). Considering the temporal evolution of the $\Delta p\text{CO}_2$ (Fig 3c) and flux over 1988-1994, the
217 rapid slowdown of $p\text{CO}_2^{\text{atmosphere}}$ growth would have caused an outgassing pulse centered on 1993

218 (Fig 1b). Beyond 1994, $p\text{CO}_2^{\text{atmosphere}}$ growth returned to approximately its long-term growth rate
219 and then grew more rapidly after 2001 (Fig 3b). Since $p\text{CO}_2^{\text{ocean}}$ lags behind $p\text{CO}_2^{\text{atmosphere}}$, $\Delta p\text{CO}_2$
220 grows more negative as the atmosphere accelerates (Fig 3b,c). For the box model forced only with
221 $p\text{CO}_2^{\text{atmosphere}}$, this increasingly negative $\Delta p\text{CO}_2$ drove a steady increase in ocean uptake from 1994
222 onward (Fig 1b).

223 This same response of the global mean air-sea CO_2 flux to $p\text{CO}_2^{\text{atmosphere}}$ forcing occurs in two
224 types of three-dimensional ocean models with constant circulation. Both an ensemble of ocean
225 hindcast models with constant climate forcing (DeVries et al., 2019) and the data-constrained
226 constant circulation Ocean Circulation Inverse Model (OCIM) (DeVries, 2014) have the same flux
227 response as in the box model forced only with variable $p\text{CO}_2^{\text{atmosphere}}$ (Fig 1b). Correlations across
228 these models are almost perfect ($r=0.97-0.98$, dashed lines in Fig 1b) and remain very high even
229 when independently detrended ($r>0.91$, Table S4). This correspondence emphasizes the critical
230 role of variability in the growth of $p\text{CO}_2^{\text{atmosphere}}$ to variability in the ocean sink. It also serves as
231 evidence that the box model is realistically estimating the timing and magnitude of this response.

232 Though it is the slowed growth of $p\text{CO}_2^{\text{atmosphere}}$ in the early 1990s that causes the mean 1990s sink
233 to be only 0.1 PgC/yr larger than the sink of the 1980s (Table S5), the pattern of the sink change
234 in the 1990s is clearly inconsistent with ocean hindcast models with variable climate (compare
235 bold green to red dash in Fig 1b), and thus is also inconsistent with the observationally-based
236 products (Fig 1a). An additional mechanism is required.

237 Volcanic eruptions of El Chichon in 1982 and Mt. Pinatubo in 1991 injected large quantities of
238 sulfate aerosols into the stratosphere and dramatically altered global air and sea surface
239 temperatures (Church et al., 2005). The forced response to these eruptions was a substantial
240 oceanic uptake of carbon and oxygen for the following 2-3 years (Eddebbar et al., 2019). Modern
241 earth system models indicate that a significant negative anomaly in global sea surface temperatures
242 (SST) was driven by the eruptions (Eddebbar et al., 2019). For the diagnostic box model, we apply
243 the same magnitude of forced global SST cooling estimated by these models, 0.1°C in 1982 and
244 0.2°C in 1991 (Fig S2) to evaluate the impact on ocean carbon sink variability.

245 With this volcano-forced SST variability applied to the box model, strong coolings in 1982 and in
246 1991 drive a rapid drop of $p\text{CO}_2^{\text{ocean}}$ (Fig 3b, solid red) and a strong uptake anomaly (Fig 1, red
247 bold). The reduced flux that would have occurred in the early 1990s due to the slowing of
248 $p\text{CO}_2^{\text{atmosphere}}$ (Fig 1b, red dash) was overwhelmed by the rapid cooling due to Mt. Pinatubo and
249 thus, a strong uptake pulse occurred (Fig 1b, red bold). The re-warming and excess DIC in the
250 surface ocean that follow Mt. Pinatubo elevates $p\text{CO}_2^{\text{ocean}}$ relative to $p\text{CO}_2^{\text{atmosphere}}$ through 2001,
251 leading to $\Delta p\text{CO}_2$ becoming less negative over this period (Fig 3c). Thus, the sink stagnates from
252 the early to late 1990s (Fig 1). The net effect of both forcings is that the reduced sink of the early
253 1990s caused by the slowed $p\text{CO}_2^{\text{atmosphere}}$ growth rate is shifted to the late 1990s by the rapid
254 cooling and slow re-warming caused by Mt. Pinatubo. In summary, the climate variability
255 mechanism that led to a neutral 1990s intra-decadal trend of the ocean carbon sink (DeVries et al.
256 2019) contains a major contribution from the ocean's response and recovery from Pinatubo
257 cooling, i.e. a response to external forcing from volcanos.

258 CO₂ fluxes from the diagnostic box model forced with both observed pCO₂^{atmosphere} and the
259 volcanoes' impacts on sea surface temperature are highly correlated to the ensemble mean of the
260 observationally-based products for their overlapping periods ($r = 0.89$, 1985-2016) and hindcast
261 models ($r=0.92$, 1980-2017) (Fig 1a, Table S4). The simplicity of these global mechanisms and
262 the strong correspondence of the resulting decadal variability to the products and the models
263 supports the conclusion that global air-sea CO₂ flux variability since 1980 has been significantly
264 driven by external forcing from (1) the changing pCO₂^{atmosphere} growth rate and (2) in the 1990s,
265 the surface ocean temperature effects of Mt. Pinatubo (Fig 4).

266 Since ocean carbon uptake is enhanced with the eruption of large volcanos, the effect on
267 pCO₂^{atmosphere} would ideally be modeled interactively. Unfortunately, land carbon sink
268 uncertainties preclude this. The sea surface temperature effects of Pinatubo led to an increased
269 ocean sink of approximately 0.5 PgC/yr (Fig.1b), but estimates of the land sink anomaly at this
270 time are much larger and uncertain, ranging 1-2 PgC/yr (Sarmiento et al. 2010; Angert et al. 2004;
271 Sarmiento 1993). In fact, the post-Pinatubo period is one of maximum uncertainty in the post-1960
272 Global Carbon Budget (Friedlingstein et al. 2019, Peters et al. 2017). Soon after the eruption of
273 Mt. Pinatubo, Sarmiento (1993) noted the coincident slowdown in growth of pCO₂^{atmosphere} and
274 reported that ¹³C records at that time suggested a terrestrial driver, while O₂/N₂ records suggested
275 an oceanic driver. A modern reconsideration of ¹³C and O₂/N₂ records may lead to better
276 understanding of this partitioning.

277 This analysis illustrates that externally forced variability played an important role in recent decadal
278 variability of the ocean carbon sink. However, the total climate variability in any variable is the
279 sum of forced variability caused by drivers external to the system, and internal variability due to
280 system dynamics (Deser et al., 2012). We have recently reviewed the many previous studies on
281 mechanisms of ocean carbon sink variability (McKinley et al., 2017). Processes discussed have
282 included the variable upper ocean circulation, wind and circulation patterns in the Southern Ocean,
283 and modes of coupled atmosphere/ocean variability in both hemispheres (DeVries et al., 2017,
284 2019; Gruber et al., 2019a; Landschützer et al., 2015, 2019; Lovenduski et al., 2007). These
285 analyses have focused on variability internal to the ocean or associated with coupled
286 atmosphere/ocean modes (McKinley et al., 2017), but have not been able to comprehensively
287 explain the global-scale decadal variability. Here, we illustrate that the observed changes can, to
288 first order, be attributed to two forcings external to the ocean.

289 Previous studies have also typically focused on a single model or a single observationally-based
290 product. However, for the best estimate of the real ocean's flux variability, it is common practice
291 to use the ensemble mean of ocean models and/or of observationally-based products
292 (Friedlingstein et al. 2019; DeVries et al., 2019; Le Quéré et al., 2018a,b), which is our approach.
293 Only the internal variability that is represented in most ensemble members will be preserved in the
294 ensemble average. Averaging damps internal variability of the individual members and thus
295 amplifies the common forced component (McKinley et al., 2016, 2017; Deser et al., 2012). Our
296 results illustrate that the current best estimate of the real ocean's flux variability, based on this
297 ensemble average, can be explained largely with forced mechanisms. However, because we do not
298 have enough information to determine which member of the ensemble best approximates the
299 ocean's true internal variability, this current best estimate potentially underestimates the full
300 impact of internal variability in the carbon sink of the real ocean.

301 What is the range of magnitude of internal variability that may be occurring in addition to the
302 forced variability that we identify? Individual observationally-based products have a range of
303 detrended flux variability from 0.14-0.30 PgC/yr, while the ensemble mean variability is 0.19
304 PgC/yr (1σ for 1985-2016). For the hindcast models, the range is 0.10-0.20 PgC/yr and the
305 ensemble mean variability is 0.11 PgC/yr for the same years. Our estimate of the amplitude of
306 externally-forced variability from the box model is 0.14 PgC/yr (Fig 1). By this measure, externally
307 forced variability as estimated by the box model is approximately equal to the total amplitude
308 common to the hindcast models, but is only about 70% of the variability common to the products.
309 On top of this, the individual models and products suggest a wide range of additional internal
310 variability. In future studies, separation of the forced component of ocean carbon sink variability
311 driven by changing $p\text{CO}_2^{\text{atmosphere}}$ and volcanos from the total variability in individual models and
312 products should help to clarify the patterns, magnitudes, and physical and biogeochemical
313 mechanisms of internal variability in the real ocean. For diagnostic (Friedlingstein et al. 2019; Le
314 Quéré et al., 2018a,b) and predictive purposes (Randerson et al., 2015) it is critical to also
315 determine which model and observationally-based estimates best represent both the internal and
316 forced variability of the real ocean.

317 Though our box model is sufficient to represent the global-mean behavior of the externally-forced
318 ocean carbon sink in recent decades, other mechanisms may increase in importance in the future.
319 As climate changes have increased impact on ocean physics and biogeochemistry, feedbacks on
320 the carbon sink of increasing magnitude can be expected. Future reduction in the overturning
321 circulation, or increased re-emergence of waters already carrying a high anthropogenic carbon load
322 would reduce the sink. A weaker biological pump would also damp net ocean carbon uptake
323 (Kwon et al. 2009). The reduced buffer capacity of the surface ocean should grow in importance
324 over time, particularly under high emission scenarios (Fassbender et al. 2017). As mitigation of
325 CO_2 emissions occurs, the growth rate of $p\text{CO}_2^{\text{atmosphere}}$ will slow. With this reduced external
326 forcing, the imprint of internal variability on the sink should become more evident. Improved
327 understanding of both internal and external mechanisms is essential to continue to accurately
328 diagnose the evolving ocean carbon sink, and to improve model-based predictions.

329 4. Conclusions

330 We have shown that externally forced variability is sufficient to explain a significant portion of
331 current model and observationally-based best-estimates of the recent decadal variability of the
332 global ocean carbon sink (Fig 1a). The reduced ocean carbon sink in the decade of the 1990s was
333 driven by a slowed growth rate of $p\text{CO}_2^{\text{atmosphere}}$. The intra-decadal timing of the slowed growth
334 rate in the 1990s was due to the surface ocean temperature response to the Mt. Pinatubo eruption
335 in 1991. Volcano-driven cooling first led to an anomalously large sink, and then as surface ocean
336 temperatures recovered, $p\text{CO}_2^{\text{ocean}}$ was elevated causing the sink to slow. In the box model, only
337 this SST response is needed to replicate the behavior of the observationally-based products and
338 the ocean hindcast models (Fig 1), but it would be of great value to perform a deeper analysis of
339 the upper ocean response to Mt. Pinatubo with future studies. From 2001 on, the recovery of the
340 global ocean carbon sink is attributable to the enhanced growth rate of $p\text{CO}_2^{\text{atmosphere}}$ (Fig 4).

341 Implications for the future ocean carbon sink are several. First, we note the relative importance of
342 external vs internal drivers of ocean sink change can be expected to change, and thus both must be

343 understood. Regarding external forcing, future large volcanic eruptions cannot be predicted, and
344 it is difficult to predict the detailed future of $p\text{CO}_2^{\text{atmosphere}}$. Thus, these are now identified as
345 additional sources of uncertainty in decadal predictions and long-term projections (Lovenduski et
346 al., 2019; McKinley et al., 2017). The timescales on which additional human interventions in the
347 climate system, such as solar radiation management or nuclear conflict, would mimic these
348 externally forced changes and modify the ocean carbon sink should be considered (Lovenduski et
349 al. 2020; Lauvset et al., 2017). Finally, since the changing growth rate of $p\text{CO}_2^{\text{atmosphere}}$ is the
350 primary driver of recent variability in the ocean carbon sink, the ocean sink should be expected to
351 slow as reductions in the $p\text{CO}_2^{\text{atmosphere}}$ growth rate occur in response to climate change mitigation
352 efforts (Peters et al., 2017). It is important that this critical feedback on the atmospheric CO_2
353 content be accurately estimated and accounted for in policy making.

354 **Acknowledgments:** Funding from many countries and agencies has supported the collection of
355 surface ocean $p\text{CO}_2$ data, for development of ocean hindcast models and observationally-based
356 products, and for international coordination. Ocean hindcast models with real climate are available
357 from <https://www.globalcarbonproject.org/carbonbudget/18/data.htm>; ocean hindcast models
358 with constant climate are available from DeVries et al. (2019); and observationally-based products
359 are available from [https://www.nodc.noaa.gov/ocads/oceans/](https://www.nodc.noaa.gov/ocads/oceans/SPCO2_1982_2015_ETH_SOM_FFN.html)
360 [SPCO2_1982_2015_ETH_SOM_FFN.html](https://www.nodc.noaa.gov/ocads/oceans/SPCO2_1982_2015_ETH_SOM_FFN.html) (SOM-FFN), [http://www.bgc-jena.mpg.de/](http://www.bgc-jena.mpg.de/CarboScope/)
361 [CarboScope/](http://www.bgc-jena.mpg.de/CarboScope/) (JENA), <https://doi.org/10.6084/m9.figshare.7894976.v1> (CSIR), and
362 <http://dods.lsce.ipsl.fr/invsat/CMEMS/> (LSCE). The code for the upper ocean box model is
363 available (<https://doi.org/10.6084/m9.figshare.11983947.v1>). G.A.M., A.R.F. and L.G. were
364 supported by NASA NNX17AK19G and by Columbia University. G.A.M., A.R.F. and N.S.L.
365 were supported by NSF OCE-1948664 and OCE-1558225. N.S.L. was also supported by NSF
366 OCE-1752724, NSF PLR-13009540, and the Open Philanthropy Project. This work would not be
367 possible without the efforts of many scientists who have collected surface ocean $p\text{CO}_2$ data and
368 contributed it to the SOCAT database, and to the developers of the observationally-based products
369 based on these data. We thank also the scientists who have contributed their ocean hindcast model
370 results to the Global Carbon Project. Leadership from the International Ocean Carbon
371 Coordinating Project (IOCCP) and the Global Carbon Project (GCP) has been essential to the
372 success of these efforts.

373

374 **References**

375

376 Angert, A., Biraud, S., Bonfils, C., Buermann, W., & Fung, I. (2004). CO_2 seasonality indicates
377 origins of post-Pinatubo sink. *Geophysical Research Letters*, 31(11).

378

379 Bakker, D. C. E., Pfeil, B., Landa, C. S., Metzl, N., O'Brien, K. M., Olsen, A., et al. (2016). A
380 multi-decade record of high-quality $f\text{CO}_2$ data in version 3 of the Surface Ocean CO_2
381 Atlas (SOCAT), *Earth Syst. Sci. Data*, 8, 383–413.

382

383 Brovkin, V., Loren, S., Jungclauss, J., Raddatz, T., Timmreck, C., Reick, C., et al. (2010).
384 Sensitivity of a coupled climate-carbon cycle model to large volcanic eruptions during
385 the last millennium. *Tellus B: Chemical and Physical Meteorology*, 62(5), 674-681.

386

- 387 Buitenhuis, E. T., Rivkin, R. B., Saille, S., & Le Quéré, C. (2010). Biogeochemical fluxes
388 through microzooplankton. *Global biogeochemical cycles*, 24(4).
- 389
- 390 Canadell, J. G., Ciais, P., Gurney, K., Le Quéré, C., Piao, S., Raupach, M. R., & Sabine, C. L.
391 (2011). An international effort to quantify regional carbon fluxes. *Eos, Transactions*
392 *American Geophysical Union*, 92(10), 81-82.
- 393
- 394 Church, J. A., White, N. J., & Arblaster, J. M. (2005). Significant decadal-scale impact of
395 volcanic eruptions on sea level and ocean heat content. *Nature*, 438(7064), 74.
- 396
- 397 Ciais, P., Sabine, C., Bala, G., Bopp, L., Brovkin, V., Canadell, J. et al. (2013). The physical
398 science basis. Contribution of working group I to the fifth assessment report of the
399 intergovernmental panel on climate change. *IPCC Climate Change*, 465-570.
- 400
- 401 Denvil-Sommer, A., Gehlen, M., Vrac, M., & Mejia, C. (2019). LSCE-FFNN-v1: a two-step
402 neural network model for the reconstruction of surface ocean pCO₂ over the global
403 ocean. *Geoscientific Model Development*, 12(5), 2091-2105.
- 404
- 405 Deser, C., Phillips, A., Bourdette, V., & Teng, H. (2012). Uncertainty in climate change
406 projections: the role of internal variability. *Climate dynamics*, 38(3-4), 527-546.
- 407
- 408 DeVries, T. (2014). The oceanic anthropogenic CO₂ sink: Storage, air-sea fluxes, and transports
409 over the industrial era. *Global Biogeochemical Cycles*, 28(7), 631-647.
- 410
- 411 DeVries, T., Holzer, M., & Primeau, F. (2017). Recent increase in oceanic carbon uptake driven
412 by weaker upper-ocean overturning. *Nature*, 542(7640), 215.
- 413
- 414 DeVries, T., Le Quéré, C., Andrews, O., Berthet, S., Hauck, J., Ilyina, T., et al. (2019). Decadal
415 trends in the ocean carbon sink. *Proceedings of the National Academy of*
416 *Sciences*, 116(24), 11646-11651.
- 417
- 418 Dickson, A. G., & Millero, F. J. (1987). A comparison of the equilibrium constants for the
419 dissociation of carbonic acid in seawater media. *Deep Sea Research Part A.*
420 *Oceanographic Research Papers*, 34(10), 1733-1743.
- 421 Dickson, A. G., Sabine, C. L., and Christian, J. R. (Eds.): Guide to Best Practices for Ocean CO₂
422 Measurements, PICES Special Publication, IOCCP Report No. 8, 2007. 8825
- 423 Dlugokencky, E.J., Thoning, K.W., Lang, P.M., Tans, P.P. (2017) NOAA Greenhouse Gas
424 Reference from Atmospheric Carbon Dioxide Dry Air Mole Fractions from the NOAA
425 ESRL Carbon Cycle Cooperative Global Air Sampling Network.
- 426
- 427 Doney, S. C., Lima, I., Feely, R. A., Glover, D. M., Lindsay, K., Mahowald, N., et al. (2009).
428 Mechanisms governing interannual variability in upper-ocean inorganic carbon system
429 and air-sea CO₂ fluxes: Physical climate and atmospheric dust. *Deep Sea Research Part*
430 *II: Topical Studies in Oceanography*, 56(8-10), 640-655.

431
432 Eddebbbar, Y. A., Rodgers, K. B., Long, M. C., Subramanian, A. C., Xie, S. P., & Keeling, R. F.
433 (2019). El Niño–Like Physical and Biogeochemical Ocean Response to Tropical
434 Eruptions. *Journal of Climate*, 32(9), 2627-2649.
435
436 Fassbender, A. J., Sabine, C. L., & Palevsky, H. I. (2017). Nonuniform ocean acidification and
437 attenuation of the ocean carbon sink. *Geophysical Research Letters*, 44(16), 8404–8413.
438
439 Fay, A. R., & McKinley, G. A. (2013). Global trends in surface ocean pCO₂ from in situ
440 data. *Global Biogeochemical Cycles*, 27(2), 541-557.
441
442 Fay, A. R., & McKinley, G. A. (2014). Global open-ocean biomes: mean and temporal
443 variability. *Earth System Science Data*, 6(2), 273-284.
444
445 Fay, A. R., Lovenduski, N. S., McKinley, G. A., Munro, D. R., Sweeney, C., Gray, A. R., et al.
446 (2018). Utilizing the Drake Passage Time-series to understand variability and change in
447 subpolar Southern Ocean pCO₂. *Biogeosciences*, 15, 3841-3855.
448
449 Friedlingstein, P., Jones, M.W., O’Sullivan, M., Andrew, R.M, Hauck, J. et al. (2019), Global
450 Carbon Budget 2019, *Earth Syst. Sci. Data*, 11(4), 1783–1838.
451
452 Frölicher, T., Joos, F., & Raible, C. (2011). Sensitivity of atmospheric CO₂ and climate to
453 explosive volcanic eruptions. *Biogeosciences*, 8(8), 2317-2339.
454
455 Gregor, L., Lebehot, A.D., Kok, S., Monteiro, P.M.S. (2019) A comparative assessment of the
456 uncertainties of global surface ocean CO₂ estimates using a machine learning ensemble
457 (CSIR-ML6 version 2019a) – have we hit the wall? *Geosci. Model Dev. Discuss.*.
458
459 Gruber, N., Gloor, M., Mikaloff Fletcher, S. E., Doney, S. C., Dutkiewicz, S., Follows, M. J., et
460 al. (2009). Oceanic sources, sinks, and transport of atmospheric CO₂. *Global*
461 *Biogeochemical Cycles*, 23(1).
462
463 Gruber, N., Landschützer, P., & Lovenduski, N. S. (2019a). The variable Southern Ocean carbon
464 sink. *Annual review of marine science*, 11, 159-186.
465
466 Gruber, N., Clement, D., Carter, B. R., Feely, R. A., Van Heuven, S., Hoppema, M., et al.
467 (2019b). The oceanic sink for anthropogenic CO₂ from 1994 to
468 2007. *Science*, 363(6432), 1193-1199.
469
470 Hauck, J., Lenton, A., Langlais, C., & Matear, R. (2018). The fate of carbon and nutrients
471 exported out of the Southern Ocean. *Global Biogeochemical Cycles*, 32(10), 1556-1573.
472
473 Jacobson, A. R., Mikaloff Fletcher, S. E., Gruber, N., Sarmiento, J. L. and Gloor M. (2007), A
474 joint atmosphere-ocean inversion for surface fluxes of carbon dioxide: 1. Methods and
475 global-scale fluxes, *Global Biogeochem. Cycles*, 21, GB1019,
476 doi:10.1029/2005GB002556

477
478 Kalnay, E., Kanamitsu, M., Kistler, R., Collins, W., Deaven, D., Gandin, L., et al. (1996). The
479 NCEP/NCAR 40-year reanalysis project. *Bulletin of the American meteorological*
480 *Society*, 77(3), 437-472.
481
482 Kwon, E. Y., F. Primeau, and J. L. Sarmiento (2009), The impact of remineralization depth on
483 the air-sea carbon balance, *Nature Geoscience*, 2(9), 630–635, doi:10.1038/NGEO612.
484
485 Landschützer, P., Gruber, N., Haumann, F. A., Rödenbeck, C., Bakker, D. C., Van Heuven, S., et
486 al. (2015). The reinvigoration of the Southern Ocean carbon sink. *Science*, 349(6253),
487 1221-1224.
488
489 Landschützer, P., Gruber, N., & Bakker, D. C. (2016). Decadal variations and trends of the
490 global ocean carbon sink. *Global Biogeochemical Cycles*, 30(10), 1396-1417.
491
492 Landschützer, P., Gruber, N., Bakker, D. C. E., & Landschützer, P. (2017). An updated
493 Observation-Based Global Monthly Gridded Sea Surface pCO₂ and Air-sea CO₂ Flux
494 Product from 1982 Through 2015 and Its Monthly Climatology. *NCEI*
495 *Accession*, 160558.
496
497 Landschützer, P., Ilyina, T., & Lovenduski, N. S. (2019). Detecting Regional Modes of
498 Variability in Observation-Based Surface Ocean p CO₂. *Geophysical Research*
499 *Letters*, 46(5), 2670-2679.
500
501 Lauvset, S. K., Tjiputra, J., & Muri, H. (2017). Climate engineering and the ocean: effects on
502 biogeochemistry and primary production. *Biogeosciences*, 14(24), 5675-5691.
503
504 Le Quéré, C., Rödenbeck, C., Buitenhuis, E. T., Conway, T. J., Langenfelds, R., Gomez, A., et
505 al. (2007). Saturation of the Southern Ocean CO₂ sink due to recent climate
506 change. *Science*, 316(5832), 1735-1738.
507
508 Le Quéré, C., Andrew, R. M., Friedlingstein, P., Sitch, S., Pongratz, J., Manning, A. C., et al.
509 (2018). Global carbon budget 2017. *Earth Syst. Sci. Data*, 10(1), 405-448.
510
511 Le Quéré, C., Andrew, R. M., Friedlingstein, P., Sitch, S., Hauck, J., Pongratz, J., et al. (2018).
512 Global carbon budget 2018. *Earth System Science Data (Online)*, 10(4).
513
514 Lovenduski, N. S., Gruber, N., Doney, S. C., & Lima, I. D. (2007). Enhanced CO₂ outgassing in
515 the Southern Ocean from a positive phase of the Southern Annular Mode. *Global*
516 *Biogeochemical Cycles*, 21(2).
517
518 Lovenduski, N. S., Gruber, N., & Doney, S. C. (2008). Toward a mechanistic understanding of
519 the decadal trends in the Southern Ocean carbon sink. *Global Biogeochemical*
520 *Cycles*, 22(3).
521

522 Lovenduski, N. S., Yeager, S. G., Lindsay, K., & Long, M. C. (2019). Predicting near-term
523 variability in ocean carbon uptake. *Earth System Dynamics*, 10(1), 45-57.
524

525 Lovenduski, N. S., Harrison, C. S., Olivarez, H., Bardeen, C. G., Toon, O. B., Coupe, J.,
526 Robock, A., Rohr, T., and Stevenson S. (2020), The Potential Impact of Nuclear Conflict
527 on Ocean Acidification, *Geophys Res Lett*, 47(3), 1535, doi:10.1007/s10584-012-0475-8.
528

529 Lucht, W., Prentice, I. C., Myneni, R. B., Sitch, S., Friedlingstein, P., Cramer, W et al. (2002).
530 Climatic control of the high-latitude vegetation greening trend and Pinatubo
531 effect. *Science*, 296(5573), 1687-1689.
532

533 McKinley, G. A., Pilcher, D. J., Fay, A. R., Lindsay, K., Long, M. C. and Lovenduski, N. S.
534 (2016), Timescales for detection of trends in the ocean carbon sink, *Nature*, 530(7591),
535 469–472.
536

537 McKinley, G. A., Fay, A. R., Lovenduski, N. S., & Pilcher, D. J. (2017). Natural variability and
538 anthropogenic trends in the ocean carbon sink. *Annual review of marine science*, 9, 125-
539 150.
540

541 Mehrbach, C., Culbertson, C. H., Hawley, J. E., & Pytkowicz, R. M. (1973). Measurement of the
542 apparent dissociation constants of carbonic acid in seawater at atmospheric pressure
543 1. *Limnology and Oceanography*, 18(6), 897-907.
544

545 Naegler, T., P. Ciais, K. Rodgers, and I. Levin (2006), Excess radiocarbon constraints on air-sea
546 gas exchange and the uptake of CO₂ by the oceans, *Geophys Res Lett*, 33(11), L11802,
547 doi:10.1029/2005GL025408.
548

549 Paulsen, H., Ilyina, T., Six, K. D., & Stemmler, I. (2017). Incorporating a prognostic
550 representation of marine nitrogen fixers into the global ocean biogeochemical model
551 HAMOCC. *Journal of Advances in Modeling Earth Systems*, 9(1), 438-464.
552

553 Peters, G. P., Andrew, R. M., Canadell, J. G., Fuss, S., Jackson, R. B., Korsbakken, J. I., et al.
554 (2017). Key indicators to track current progress and future ambition of the Paris
555 Agreement. *Nature Climate Change*, 7(2), 118.
556

557 Randerson, J. T., Lindsay, K., Munoz, E., Fu, W., Moore, J. K., Hoffman, F. M., et al. (2015).
558 Multicentury changes in ocean and land contributions to the climate-carbon
559 feedback. *Global Biogeochemical Cycles*, 29(6), 744-759.
560

561 Reynolds, R. W., Rayner, N. A., Smith, T. M., Stokes, D. C., & Wang, W. (2002). An improved
562 in situ and satellite SST analysis for climate. *Journal of climate*, 15(13), 1609-1625.
563

564 Rödenbeck, C., Keeling, R. F., Bakker, D. C., Metzl, N., Olsen, A., Sabine, C., & Heimann, M.
565 (2013). Global surface-ocean p (CO₂) and sea-air CO₂ flux variability from an
566 observation-driven ocean mixed-layer scheme.
567

568 Rödenbeck, C., Bakker, D. C., Gruber, N., Iida, Y., Jacobson, A. R., Jones, S., et al. (2015).
569 Data-based estimates of the ocean carbon sink variability—first results of the Surface
570 Ocean pCO₂ Mapping intercomparison (SOCOM). *Biogeosciences*, 12, 7251-7278.
571

572 Sarmiento, J. L. (1993), Carbon-Cycle - Atmospheric CO₂ Stalled, *Nature*, 365(6448), 697–698.
573

574 Sarmiento, J. L., & Gruber, N. (2006). *Ocean biogeochemical dynamics*. Princeton University
575 Press.
576

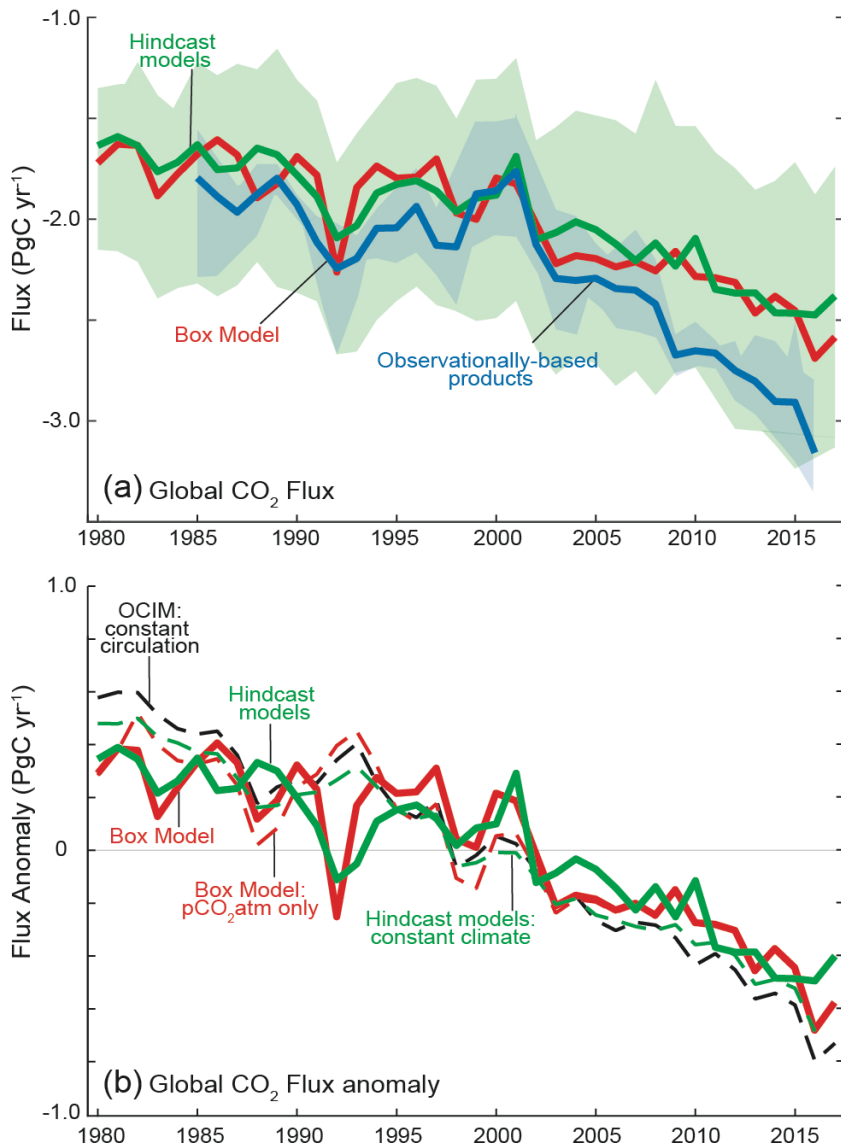
577 Sarmiento, J. L., Gloor, M., Gruber, N., Beaulieu, C., Jacobson, A. R., Mikaloff Fletcher, S. E.,
578 et al. (2010). Trends and regional distributions of land and ocean carbon
579 sinks. *Biogeosciences*, 7(8), 2351-2367.
580

581 Schwinger, J., Goris, N., Tjiputra, J. F., Kriest, I., Bentsen, M., Bethke, I., et al. (2016).
582 Evaluation of NorESM-OC (versions 1 and 1.2), the ocean carbon-cycle stand-alone
583 configuration of the Norwegian Earth System Model (NorESM1). *Geoscientific Model
584 Development*, 9, 2589-2622.
585

586 Séférian, R., Delire, C., Decharme, B., Voldoire, A., y Melia, D. S., Chevallier, M., et al. (2016).
587 Development and evaluation of CNRM Earth system model—CNRM-ESM1.
588

589 Takahashi, T., S. Sutherland, R. Wanninkhof, C. Sweeney, R. Feely, D. Chipman, B. Hales, G.
590 Friederich, F. Chavez, and C. Sabine (2009), Climatological mean and decadal change in
591 surface ocean pCO₂, and net sea–air CO₂ flux over the global oceans, *Deep-Sea
592 Research Part II*, 56(8-10), 554–577.
593

594 Wanninkhof, R. (2014) Relationship between wind speed and gas exchange over the ocean
595 revisited. *Limnology and Oceanography: Methods*, 12(6):351-362.
596

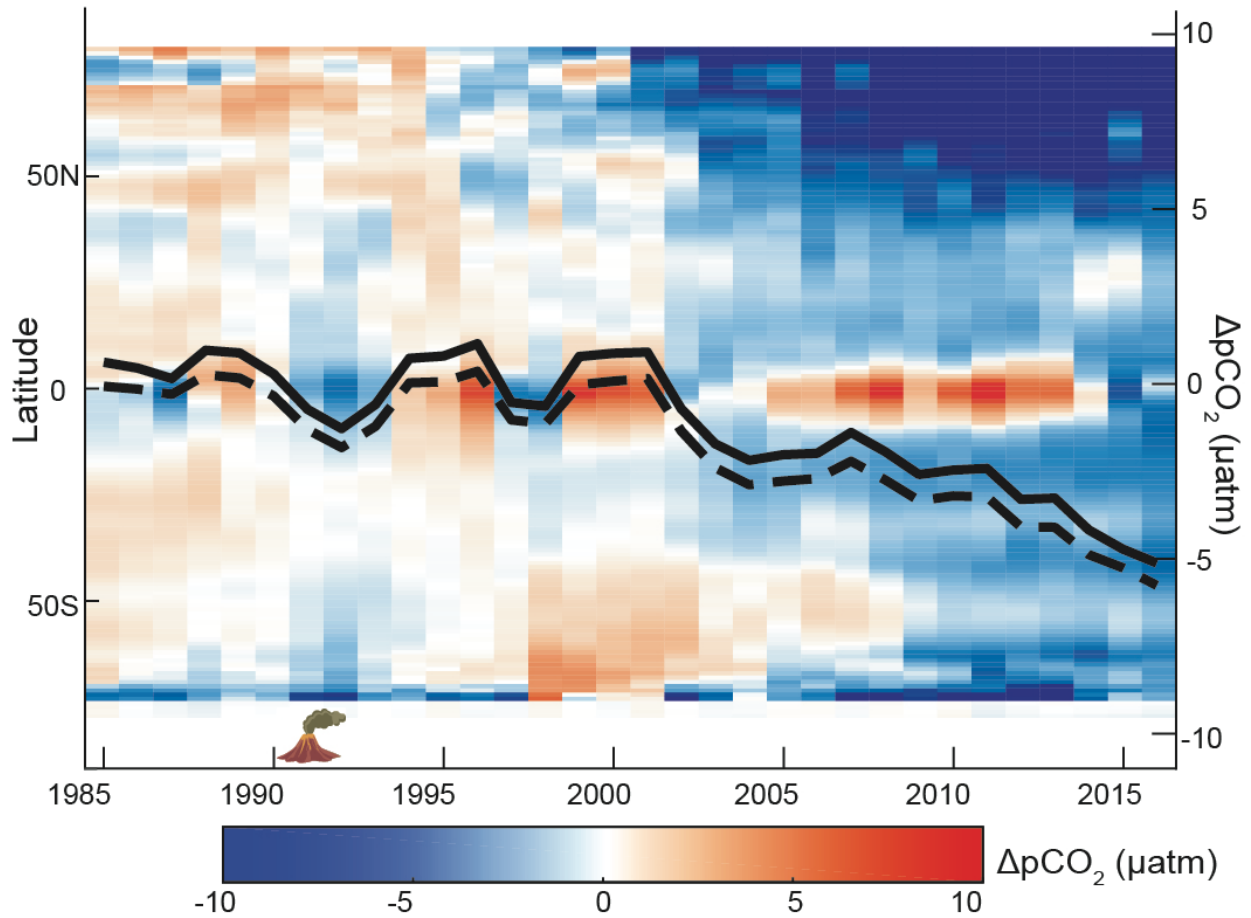


598

599 **Fig 1: Air-sea CO₂ flux of anthropogenic carbon** from observationally-based products (blue),
 600 hindcast models (green) and upper ocean diagnostic box model (red); negative flux into the
 601 ocean. (A) global (bold), with range of individual members (shading), (B) anomalies of air-sea
 602 CO₂ flux for the hindcast models with constant climate and variable pCO₂^{atmosphere} (green
 603 dashed), and variable climate and variable pCO₂^{atmosphere} (solid green); box model with only
 604 pCO₂^{atmosphere} forcing (dashed red) and both pCO₂^{atmosphere} and volcano-driven SST forcing (solid
 605 red); and the constant circulation Ocean Circulation Inverse Model (dash black, DeVries et al.
 606 2014) that imposes variable pCO₂^{atmosphere}. In B, dashed lines are correlated at 0.97-0.99 and the
 607 solid lines 0.92 (Table S4). In A, the mean flux of the observationally-based products is
 608 increased by 0.45 PgC/yr (Jacobson et al. 2007) to account for the outgassing of natural carbon
 609 supplied by rivers to the ocean.

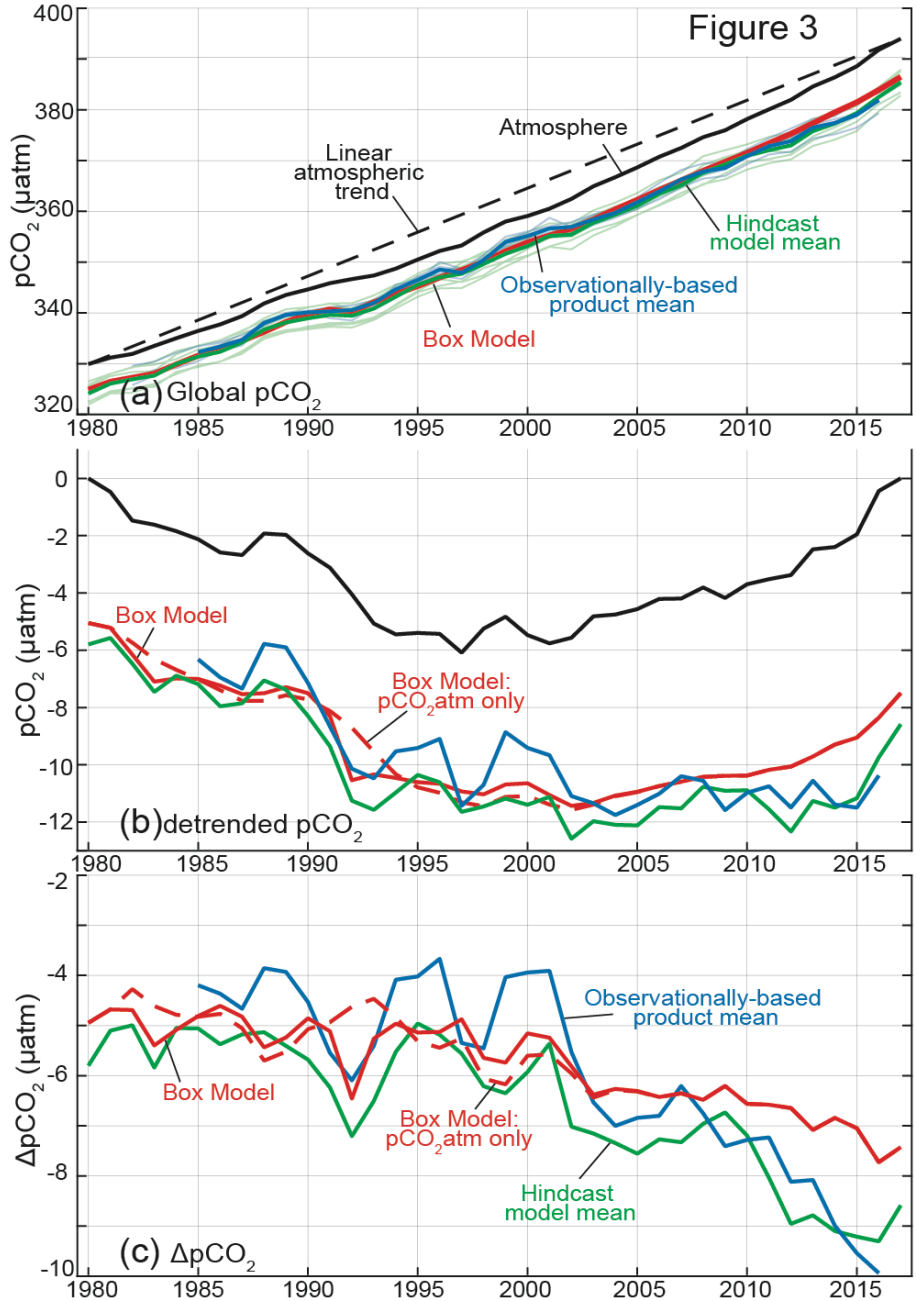
610

Figure 2



611

612 **Fig 2: Latitudinal mean anomaly $\Delta p\text{CO}_2$ (μatm)** from the ensemble mean of the
613 observationally-based products. Anomaly is calculated from the 1990-1999 mean. Annual
614 $\Delta p\text{CO}_2$ time series overlaid in black for global (solid) and global excluding east equatorial
615 Pacific biome (dashed).
616



617

618 **Fig 3: Trends of $p\text{CO}_2^{\text{atmosphere}}$ (black) and $p\text{CO}_2^{\text{ocean}}$ (colors) (A) with trend, (B) detrended**
 619 **with the long-term $p\text{CO}_2^{\text{atmosphere}}$ trend (1.70 $\mu\text{atm}/\text{yr}$ from 1980 to 2017), (C) $\Delta p\text{CO}_2$ (=**
 620 **$p\text{CO}_2^{\text{ocean}} - p\text{CO}_2^{\text{atmosphere}}$).** Observationally-based products mean (blue), hindcast model mean
 621 (green) and upper ocean diagnostic box model (red). The box model is forced with only
 622 $p\text{CO}_2^{\text{atmosphere}}$ (dashed) and with both $p\text{CO}_2^{\text{atmosphere}}$ and volcano-associated SST change (solid).
 623 Hindcast models without the water vapor correction applied to their atmospheric $p\text{CO}_2$ time
 624 series are corrected to account for that difference. Fig S6 expands on these results by including
 625 additional box model forcing scenarios.

Figure 4



626

627 **Fig 4: Mechanisms of recent decadal variability of the ocean carbon sink.** (A) The reduced
628 sink of the 1990s (black arrow) was due to a slowing of the $p\text{CO}_2^{\text{atmosphere}}$ growth rate, and the
629 rapid cooling and slower warming recovery in response to the eruption of Mt. Pinatubo (red
630 arrows). (B) In the 2000s and beyond, $p\text{CO}_2^{\text{atmosphere}}$ growth accelerates, leading to enhanced
631 $\Delta p\text{CO}_2$ and sink growth.

632